Journal of ELECTRONIC MATERIALS, Vol. 41, No. 5, 2012
DOI: 10.1007/s11664-012-2020-y
© 2012 TMS

Coalescence of InP Epitaxial Lateral Overgrowth by MOVPE with V/III Ratio Variation

NICK JULIAN,[1,3] PHIL MAGES,[1,4] CHONG ZHANG,[1] JACK ZHANG,[2] STEPHAN KRAEMER,[2] SUSANNE STEMMER,[2] STEVEN DENBAARS,[1,2] LARRY COLDREN,[1,2] PIERRE PETROFF,[1,2] and JOHN BOWERS[1,2]

1.—Department of ECE, University of California Santa Barbara, Santa Barbara, CA 93106, USA. 2.—Department of Materials, University of California Santa Barbara, Santa Barbara, CA 93106, USA. 3.—e-mail: njulian@engineering.ucsb.edu. 4.—e-mail: pmages@ece.ucsb.edu

The effects of V/III ratio and seed window orientation on the coalescence of epitaxial lateral overgrowth InP over SiO_2 using metal organic vapor-phase epitaxy with tertiary butyl phosphine were investigated. Parallel lines having $\theta = 60°$ and 30° off $[0\bar{1}1]$ were coalesced, and their lateral growth rate variation with V/III was measured. Coalescence of lines separated by narrow angles in a star-like pattern was also studied. We find the greatest extent of coalescence to occur when the window stripe is oriented just off of the $\langle 010 \rangle$ directions. V/III ratio strongly affects the extent of coalescence, showing an alternating enhancement or inhibition depending on which side of the $\langle 010 \rangle$ direction the stripes are oriented. The variation in quality of coalesced material between stripes separated by narrow angles is examined with cross-sectional transmission electron microscopy, illustrating the most problematic growth directions under two V/III ratio conditions.

Key words: Metal organic vapor-phase epitaxy (MOVPE), metal organic chemical vapor deposition (MOCVD), OMVPE, selective-area growth (SAG), epitaxial lateral overgrowth (ELO), coalescence, heteroepitaxy

INTRODUCTION

Indium phosphide (InP) plays a significant role in modern photonic devices. Its heteroepitaxial integration onto silicon would yield significant improvements in the cost and efficiency of optoelectronic integrated circuits intended for use in the computing and telecommunications industries. A promising method for realizing such material integration is epitaxial lateral overgrowth (ELO). In this method a growth-inhibiting layer is patterned with windows opening to the substrate, forcing growth into a limited area until protruding out of the windows, at which point it is then able to propagate laterally with the hope of coalescing with neighboring lateral growths. There are then two significant sources for defects to appear in the grown layer. Defects may propagate through the mask openings, or they may also be generated during coalescence. We limit this study to homoepitaxial ELO of InP on InP substrates to explore methods of maximizing the area of defect-free overgrowth as well as minimizing coalescence-related defects with respect to ELO mask design and growth conditions. This restriction to homoepitaxy allows us to be certain that any defects present in the grown material are due solely to phenomena associated with lateral overgrowth, coalescence, and interaction with the ELO mask. The stress fields and defects arising from thermal and lattice mismatch with a Si substrate, which would vary with seed layer thickness, composition, and defect density, would introduce uncertainty when attempting to attribute defect formation purely to mask design and growth conditions. We observed that variations

Presented at EMC 2011, University of California Santa Barbara June 22–24, 2011.
(Received August 15, 2011; accepted February 16, 2012; published online March 22, 2012)

in window stripe direction had the most profound effect on sidewall morphology, demonstrating two classes of stripe orientation near ⟨010⟩ having fast lateral growth, which respond in distinct ways to changes in V/III precursor partial pressure ratio.

In this paper we describe the results of ELO growth and coalescence using two categories of mask pattern: parallel stripes and a star-like configuration of 32 intersecting arms separated by 5.625°. Special note is taken of the morphological variation of growth through stripes oriented just off of the ⟨010⟩ family of directions with V/III ratio, and our use of these variations to achieve lateral coalescence. We attribute the morphological variations primarily to the growth rate anisotropies of the facets involved, and note the introduction of capillary mass transport within regions undergoing coalescence. We present cross-sectional transmission electron microscopy (TEM) images of coalesced material between ranges of stripe orientations separated by narrow angles in a star-like configuration to evaluate their quality.

EXPERIMENTAL PROCEDURES

To create the mask patterns for ELO growth, we first deposited approximately 200 nm of SiO_2 via plasma-enhanced chemical vapor deposition (PECVD) at 250°C with a low deposition rate. We then applied a thin (20 nm) layer of chromium, upon which we defined the contours of our ELO windows using conventional photolithography. Inductively coupled plasma (ICP) etching was used to first etch the windows into chromium, then photoresist was removed. ICP etching was used again to open the windows into SiO_2, and then to selectively remove the remaining chromium. This hard-mask process minimizes contamination from polymerized photoresist, which otherwise tends to stick to the InP and SiO_2 surfaces after the initial ICP etching. Before growth, the native InP oxide was removed with a dip in undiluted 90 wt.% to 98 wt.% sulfuric acid, followed by a short rinse in deionized water.

Growth was then carried out on (100) InP substrates in a 2-inch horizontal metal organic vapor-phase epitaxy (MOVPE) reactor using trimethylindium (TMI) and tertiary butyl phosphine (TBP) precursors and hydrogen as carrier gas at 350 Torr and 615°C. This growth temperature was experimentally determined to minimize unwanted nucleation on our particular SiO_2 surfaces. Partial pressures of TBP were varied from 0.22 Torr to 4.1 Torr, yielding V/III ratios ranging from 50 to 496 and growth rates between 0.5 Å/s and 8 Å/s. However, growth rates faster than 4 Å/s were seen to increase chaotic variations in the growth morphology. All growths in this study were thus limited to a rate of 4 Å/s or less. Due to the lower pressure limit of our reactor, this restricts us to V/III ratios greater than or equal to 124.

Analysis was performed using scanning electron microscopy and cross-sectional TEM. The cross-sectional TEM samples were prepared using a focused ion beam (FIB) to excavate and thin the regions of interest into lamellae of approximately 200 nm thickness.

RESULTS

Morphological Characteristics and Variation with V/III Ratio

A striking feature of the resulting growth over star-like patterns was their variation with stripe direction. In Fig. 1 we see two of these samples grown with V/III ratios of 124 and 248, where the growth of arms through windows oriented along the ⟨010⟩ directions is unlike its neighbors. These ⟨010⟩ arms have large stable facets, while the growth through windows on either of their sides has regions in which coalescence has progressed outward from the center of the star. This coalescence extends a shorter distance for angles further away from the ⟨010⟩ arms. It is also apparent from Fig. 1 that the widths of the arms nearest $[0\bar{1}0]$ increase with distance from the pattern center, and to a slightly greater extent than the arms farthest from $[0\bar{1}0]$.

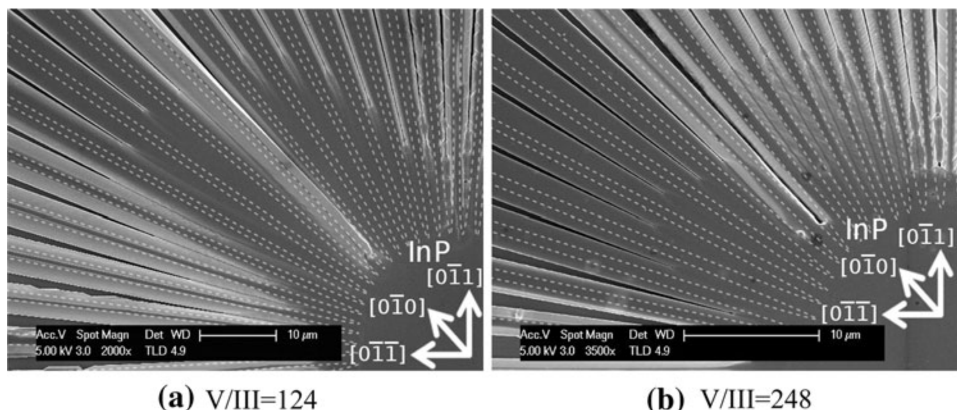

Fig. 1. Overview of coalescence behavior with variations in direction and V/III ratios of (a) 124 and (b) 248. Dashed lines outline the overgrown boundaries of 0.8-μm-wide windows through which growth initiated.

This may be attributed to a growth rate enhancement from the widening SiO_2 mask. Such growth rate enhancements occur when precursors diffuse from the SiO_2 mask onto a preferred growth facet.[1] For the lower V/III ratio of 124, arms rotated toward $[0\bar{1}1]$ away from $[0\bar{1}0]$ ($\theta < 45°$ when measured from $[0\bar{1}1]$) show a greater angular range of complete coalescence, whereas fewer of the arms rotated toward $[0\bar{1}\bar{1}]$ ($\theta > 45°$) have fully coalesced. These contrasting effects are reversed when the V/III ratio is increased to 248. Under this condition, the coalescence of a greater number of arms toward $[0\bar{1}\bar{1}]$ ($45° < |\theta| < 90°$) advanced, while coalescence of the arms rotated toward $[0\bar{1}1]$ ($\theta < 45°$) was incomplete. In addition, at this magnification we can see that the sidewalls of these two groups of arms differ. A closer view of the parallel stripes shown in Fig. 2 illustrates in greater detail the morphological differences between the arms of these two directional groups and their response to V/III variation. For $\theta = 30°$ we see sidewalls consisting of jagged steps, which we refer to as a "fillet" character for convenience. These steps appear to contain {101} and (111)A facets, as highlighted on the inset rhombicuboctahedron which shows all low index facet families for zincblende crystals that could be visible in this view. For growths neighboring $[0\bar{1}0]$ with $|\theta| < 45°$, an increase in V/III ratio causes the top (100) facet to be narrower, with taller fillet sidewalls. For growths neighboring $[0\bar{1}0]$ with $45° < |\theta| < 90°$ we see smooth sidewalls which transform into an overhanging ledge when the V/III ratio is raised from 124 to 248. For this direction, there are no obvious low-index facet formations other than (100). We refer to these as having "dovetail" character.

Lateral Growth of Parallel Stripes

We then investigated lateral growth of parallel stripes from each of the two directional classes: 30° off of $[0\bar{1}1]$ with fillet character and 60° off of $[0\bar{1}1]$ with dovetail character. For both categories, the lateral growth of stripes separated by 2.5 μm slowed as the total open field thickness (OFT) growth was increased, as shown in Fig. 3a, b. Only the growths of dovetail character along 60° achieved coalescence over a 2.5-μm spacing for either V/III ratio. The lateral growth rate of this orientation also increased significantly with increasing V/III ratio, achieving coalescence with as little as 0.9 OFT (marked by a star in Fig. 3b) when using V/III of 409. The absolute TBP pressure was held constant for each of these except for the rightmost point of Fig. 3b. The plot of lateral growth versus V/III ratio in Fig. 3c shows that lateral growth for both stripe directions

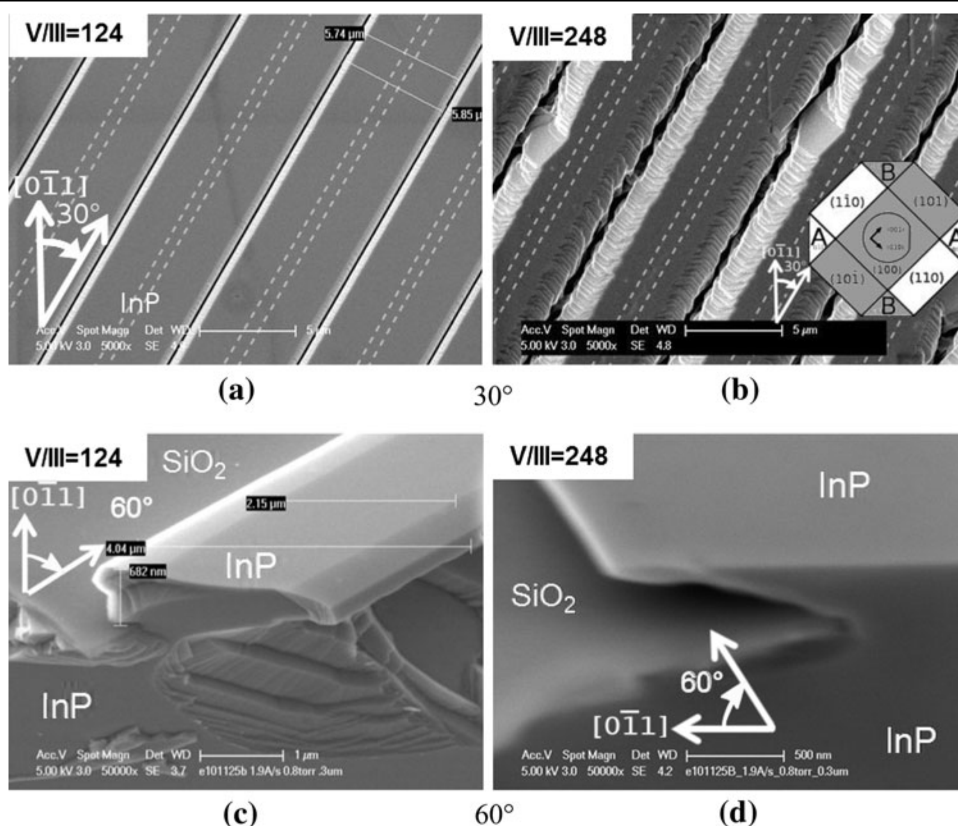

Fig. 2. Morphological variation of stripes oriented 30° (a, b) and 60° (c, d) with V/III ratios of 124 (a, c), and 248 (b, d). The inset of (b) highlights on a rhombicuboctahedron the facet planes nearest the sidewalls of 30° stripes. Dashed lines outline the overgrown 0.8-μm-wide ELO mask openings.

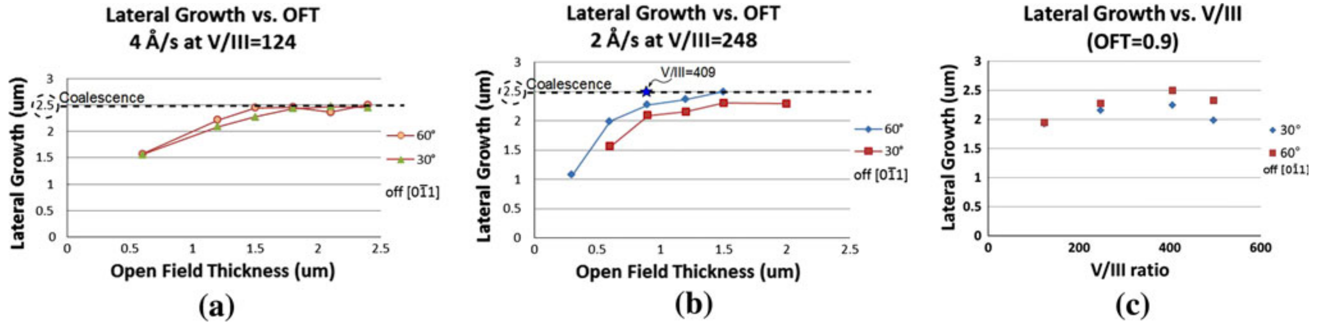

Fig. 3. Lateral growth of parallel stripes separated by 2.5 μm of SiO_2 for (a) V/III = 124, (b) V/III = 248, and (c) variation with V/III ratio.

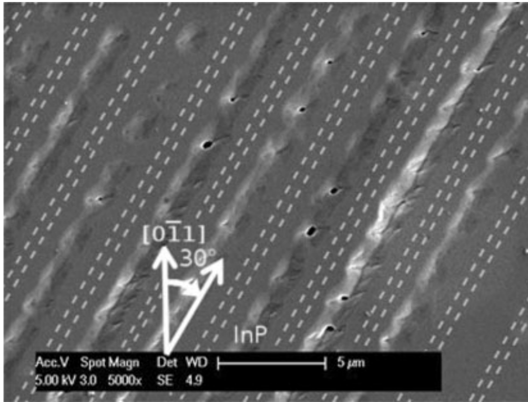

Fig. 4. Multipoint two-zipper-mode coalescence of parallel stripes 30° off of [0$\bar{1}$1] having small SiO separation. Dashed lines outline the overgrown 0.8-μm-wide ELO mask openings.

incurs maximal enhancement between V/III ratios of 248 and 406, while this enhancement is less effective for orientations 30° off of [0$\bar{1}$1] (fillet sidewalls) than for orientations 60° off of [0$\bar{1}$1] (dovetail). The difference between the two increases monotonically with V/III, and the enhancement of 30° stripes ceases with V/III of 496.

Behavior During Coalescence

The coalescence behavior of parallel stripes 30° off of [0$\bar{1}$1] is captured in Fig. 4. Here coalescence is initiated at multiple points, over a narrower mask separation than reported above, and proceeds in what Yan et al. term a two-zipper mode with high likelihood of forming defects when coalescence completes and the voids shown finally close.[2]

Introducing a nonzero angle between growth fronts helps to avoid this two-zipper coalescence, as shown previously in Fig. 1, allowing what Yan[2] denotes as a one-zipper coalescence mode. Looking more closely at the coalescence taking place between these arms separated by 5.625°, shown in Fig. 5, helps to illustrate the evolution of one-zipper coalescence. For the directions having fillet sidewalls, specifically between arms having θ = 39.375° and 33.75°, we see that coalescence is initiated from the bottom of the growth for V/III ratios of both 124 and 248 in Fig. 5a, b. The surface morphology of the coalescent region in both cases is noticeably different from the nearby fillet steps. As coalescence proceeds up toward the top surface, this less jagged shape begins to consume more area than the large steps. For both V/III ratios we see that the steps become curved. For the lower V/III of 124 the steps yield to the new coalescent surface without recourse. For higher V/III of 248 the steps initially yield to the smoother morphology, but return at least once more further into the circle before they disappear entirely.

Examining the analogous coalescent regions for directions having smooth sidewalls, or dovetail character, we see in Fig. 5c, d that coalescence proceeds from the bottom surface to the top for V/III of 124, a behavior shared with the fillet sidewall directions. However, in this case the separation between sidewalls near the top (100) surface in the region of coalescence is not as wide. For V/III of 248 the coalescence does not appear to initiate from below at the mask surface, but coalescence is only visible along the top (100) surface.

Cross-Sectional TEM

To examine the quality of coalesced material we present cross-sectional TEM images in Fig. 6b–d. The dark lines shown in the sample overview TEM (Fig. 6b) can be assigned to bending contours resulting from the curvature of this 20-μm-long 200-nm thin lamellae as it is suspended by opposite ends. Figure 6a shows the region to be examined as it was being prepared by FIB. This region covers the coalescence of several stripe pairs separated by narrow angles of 5.625°, specifically those having $28.125° < |\theta| < 67.5°$, which includes areas containing both fillet and smooth sidewall characteristics. Two layers of platinum were initially deposited over the regions of interest to protect them from the ion beam. For V/III of 124, in Fig. 6c, we see a coalescence-related defect between arms rotated 61.875° and 56.25° away from [0$\bar{1}$1], corresponding to the coalescence behavior of smooth sidewall growths shown in Fig. 5c. In contrast we do not yet see any defects forming between the two sets of arms within the angular range of 28.125° to 39.375°

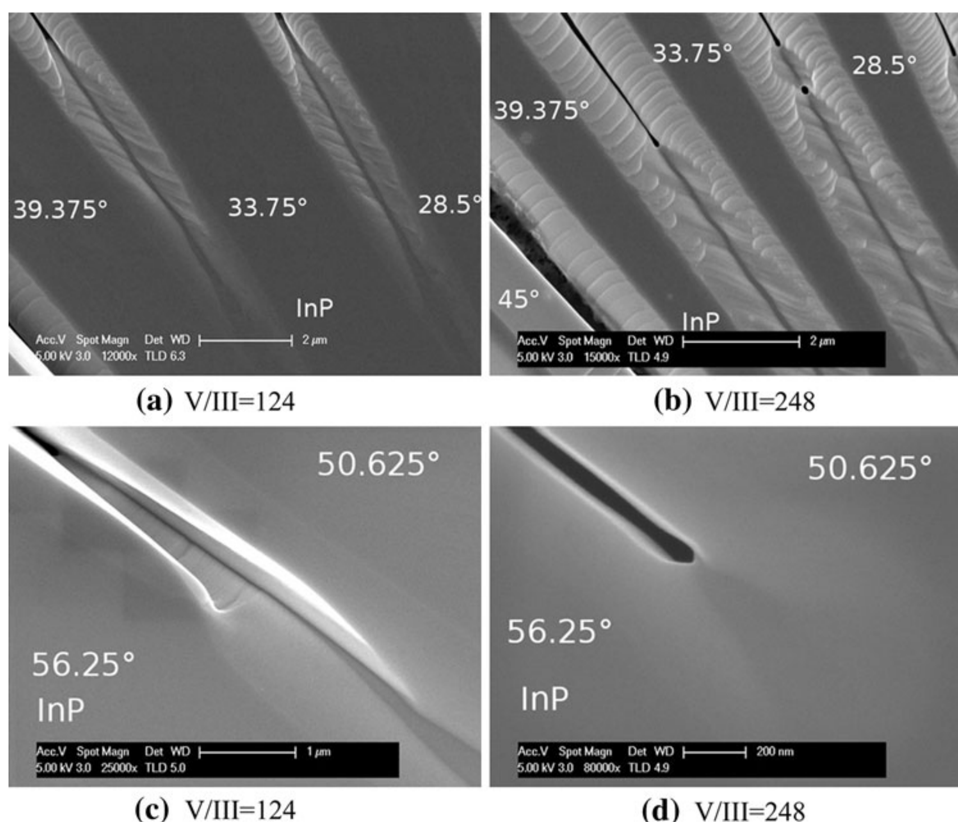

Fig. 5. Coalescence regions between arms oriented (a, b) 39.375°, 33.75°, 28.5° and (c, d) 56.25°, 50.625° off of [0$\bar{1}$1], for V/III ratios of (a, c) 124, and (b, d) 248. Images (c, d) are at higher magnification due to smaller feature size.

for this lower V/III ratio, as shown in Fig. 6d, corresponding to orientations having jagged or fillet sidewalls. Figure 6e–g shows TEM images of a similar lamella grown with higher V/III ratio of 248. Here we notice a defect within coalescence of fillet-style sidewalls. This appears to be a dislocation which originated at the junction of neighboring fillet sidewalls. The coalescence of dovetail sidewalls does not show any obvious defects for this higher V/III ratio, although they do introduce spacious voids directly below coalescence due to their dovetail cross-sectional shape.

DISCUSSION

Morphological Characteristics and Variation with V/III Ratio

To maximize the useful area of material grown via ELO, it is desirable to maximize the extent of lateral overgrowth per OFT growth, and to optimize the quality of material at coalescence regions. We have demonstrated a correlation of these two features with growth morphology, and their response to V/III ratio adjustment. It is therefore useful to investigate the mechanisms causing these morphological variations for future optimization.

It was noted in a previous section that the steps along sidewalls of fillet category, present only on stripes just off of ⟨010⟩ having $|\theta| < 45°$ measured from the [0$\bar{1}$1] direction, contain planes appearing to be {101} and (111)A facets, as seen in Fig. 2b. In contrast, the stripes having $45° < |\theta| < 90°$ did not show such low-index facet formation on their upper sidewalls. The following question arises: Why do the slow-growing (111)B facets not appear on the lateral growth sidewalls, while the fast-growing (111)A facets fail to congeal with neighboring {101} facets to form a smooth high-index plane sidewall?

Following Asai and others, we offer a speculative explanation of this morphological phenomenon using a dangling bond model.[3,4] As is usual, we assume that, once an indium atom incorporates onto a site, its dangling bonds are swiftly occupied by phosphorus due to excess supply. Growth is then limited by indium incorporation, the rate of which is subject to precursor decomposition anisotropies of the different crystallographic planes and surface diffusion of indium atoms along the local chemical potential gradient ("capillarity"), which is linearly dependent on the surface free energy.[5–7] Figure 7 shows each of the configurations of atomic planes involved, including both concave and convex intersections of step facets. At each site of possible indium atom incorporation is a number quantifying the total change in dangling bonds if an indium atom were to attach there. Negative change in the number of dangling bonds represents a reduction in surface energy upon indium incorporation, and

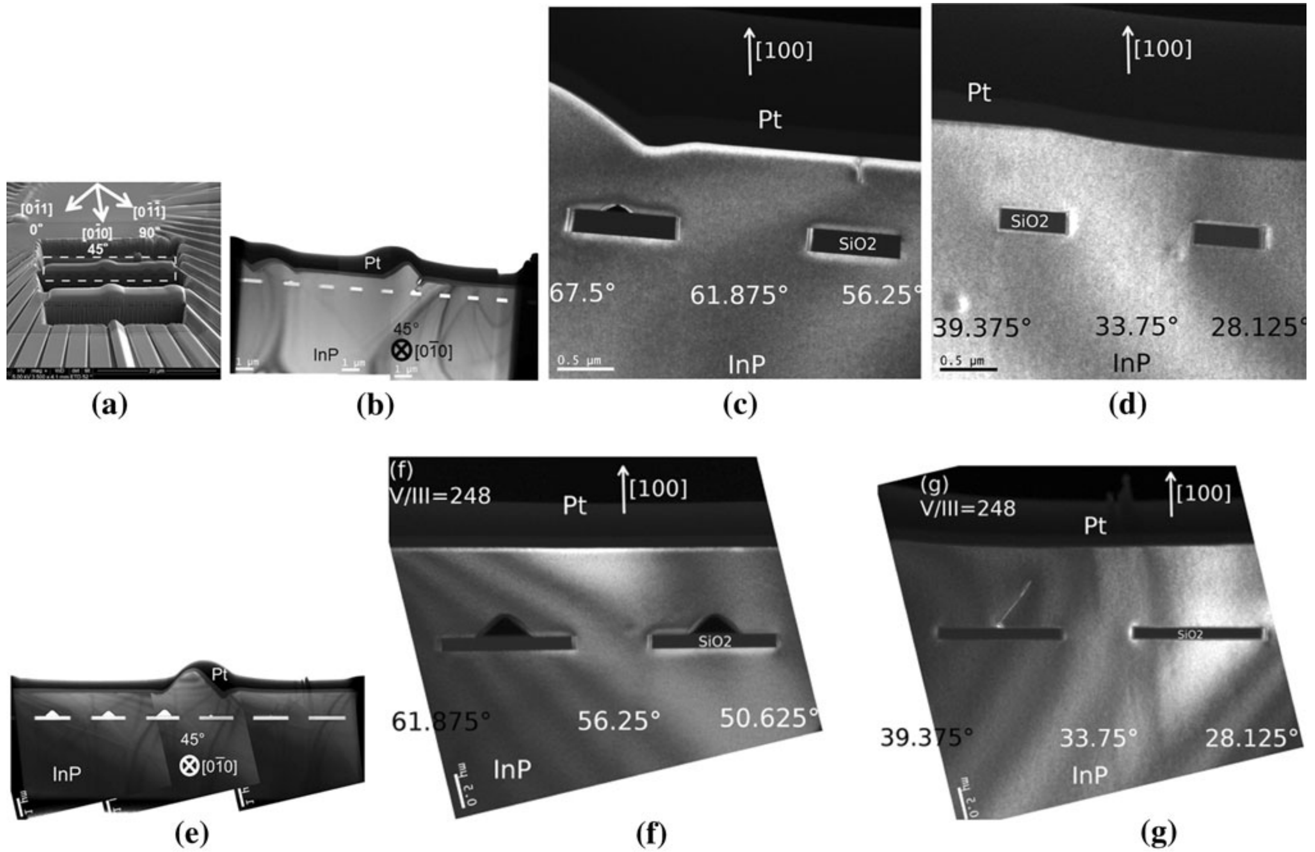

Fig. 6. (a) Location of lamellae to be examined on star-like pattern, after initial excavation. Bright-field TEM overview of lamellae for V/III ratios of (b) 124 and (e) 248. Dark-field TEM of coalesced regions showing defect locations for V/III of 124 (c, d) and 248 (f, g). Triangular dark areas in (f) correspond to voids which do not fill once formed.

positive change represents a potential energy barrier for incorporation.

A possible explanation to our question could be found by looking near the kink sites where planes intersect, marked by grey circles in Fig. 7. The concave intersection of (111)B with the relevant {110} plane contains an energetically favorable site for indium incorporation, having a dangling bond change of −2, while indium incorporation at the convex intersection is energetically inhibited by a dangling bond change of +2. Such an arrangement encourages minimization of (111)B facet step height and the appearance of a macroscopically smoother surface for $45° < \theta < 90°$. In contrast, the kink sites at both intersections of (111)A and (110) surfaces are energetically unfavorable compared with sites elsewhere on the (111)A surface. This contributes to the preferred growth and maintenance of the (111)A planes, as observed, and may contribute to inhibition of capillarity or mass transport effects between these two planes at this temperature.

A consequence of our analysis is that growth of arms with fillet sidewall character progresses laterally through the flow of very large steps consisting of (111)A facets flowing over neighboring {101} facets.

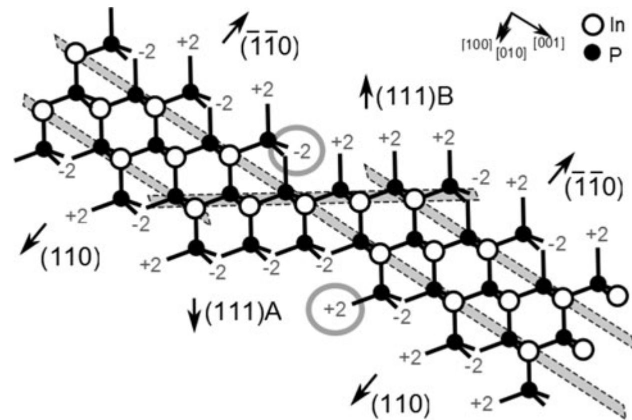

Fig. 7. Ball-and-stick model of the atomic configuration, with change in dangling bonds noted for relevant intersections of ($\bar{1}\bar{1}$0), (111)B, (111)A, and (110) planes.

Before resuming the analysis of our growths, it is desirable to propose a hierarchy of growth rates amongst low-index facets. Growth on (111)A planes is often reported as the most substantial, while (111)B planes usually show very little growth.[5,8] On the {110} faces the dangling bond change alternates between +2 and −2 between neighboring locations.

This mixture decreases the likelihood of In incorporation, and thus {110} faces should grow more slowly than (111)A planes. Sun[4] uses a dangling bond theory to argue that, under high V/III ratio, {110} facets have higher growth rates than (100) facets in hydride vapor-phase epitaxy (HVPE). They attribute this to energetically favorable initiation of each {110} layer at the intersection of {110} and (100). Thus, the theoretical hierarchy of facet growth preference under high V/III ratio, from highest to lowest, is: (111)A, {110}, (100), and lastly (111)B.

Coalescence

In a previous section it was demonstrated that the extent to which coalescence completes between stripes separated by 5.625° on a star-like pattern is dependent on the V/III ratio (Fig. 1). In particular, those oriented less than 45° off of $[0\bar{1}1]$ were coalesced to a greater extent than those oriented with $45° < \theta < 90°$ off of $[0\bar{1}1]$ for a lower V/III ratio of 124, while these roles were reversed for V/III of 248. This may be partially attributed to the preferential step flow directions of growth on the (100) facet demonstrated by Asai et al.[3] Step flow in the $[0\bar{1}1]$ direction on the (100) plane is essentially constant for a wide range of V/III, as is the cumulative vertical growth, while step flow in the [011] direction is slower than $[0\bar{1}1]$ for low V/III, and faster than $[0\bar{1}1]$ for higher V/III.

For higher V/III this correlates with greater lateral growth of stripes with $45° < \theta < 90°$ off $[0\bar{1}1]$, as explained in the previous section. Due to the flat top and sharp sidewalls of these dovetail stripes, coalescence of a small region is completed very soon after initiation and the space between neighboring arms fills completely. For $\theta < 45°$, having fillet sidewalls, faster $[0\bar{1}1]$ step flow direction on the (100) plane correlates with faster {101} plane growth, whose vertical expansion inherently opposes complete coalescence by expanding the gap between the tops of the arms. The lengthening of {110} planes requires taller (111)A steps to conform to the angle of the growth stripe.

For lower V/III ratio, {110} layer initiation at the upper intersection with (100) slows, and thus so does the entire {110} growth rate. For $45° < \theta < 90°$, this eliminates the overhanging dovetail growth, resulting in less lateral extension and forcing coalescence to initiate at the bottom of the sidewall. A defect may then be formed as seen in Fig. 6c when the top and bottom of opposite arms simultaneously converge. For $\theta < 45°$, lower {110} growth preference enhances the deposition on the (111)A step faces while decreasing the vertical growth rate. This results in lower fillet sidewall heights, and thus coalescence proceeding from the bottom up would complete sooner.

The coalescence of parallel stripes at $\theta = 30°$ away from $[0\bar{1}1]$, those having fillet sidewalls, was likely inhibited by the decrease in growth rate enhancement due to decreased precursor flux from the diminishing SiO_2 mask area between growth fronts, a mechanism noted by Kayser et al.[1] In contrast, the coalescence of stripes 60° away from $[0\bar{1}1]$, having a dovetail profile, was not as inhibited by this effect at high V/III ratio. This may be attributed to the decreasing area of preferred growth surface on the sidewall, requiring the incorporation of fewer and fewer atoms per lateral growth distance, the supply of which was enhanced by the preference for step flow on the (100) surface toward the [011] direction at high V/III ratio.[3]

It is important to note in Fig. 5 that the (111)A facets on each step near the coalescence region have shrunken and appear to curve toward (100) at the top, and either (011) or $(0\bar{1}\bar{1})$ at the bottom. This phenomenon is also seen further away from coalescent regions, but is far less pronounced. In these regions where (111)A intersects with (100) or any region neighboring coalescence, we cannot rule out capillarity or mass transport effects involving the (111)A plane. The introduction of coalescent surfaces between arms changes the chemical potential profile, influencing the balance between capillary mass transport and facet growth rate anisotropies,[5,7,9] and thus may be causing the curvature of the steps. The defects, or lack thereof, seen under TEM in Fig. 6d, h for fillet sidewall growths ($|\theta| < 45°$ off $[0\bar{1}1]$) are indicative of the need to balance growth rate anisotropies of facets with capillary mass transport to achieve optimal material. It is likely that the defect of Fig. 6g resulted from two-zipper growth mode occurring after two opposing (111)A facets collided. The lack of defect in Fig. 6d indicates sufficient capillary mass transport to avoid such colliding facets. This demonstrates an alternation between facet growth dominance and capillary mass transport dominance by V/III ratio adjustment.

CONCLUSIONS

We have demonstrated coalescence of ELO-grown InP between sidewalls of two types, and their variation with V/III ratios ranging from 124 to 496. Parallel lines oriented $\theta = 60°$ off $[0\bar{1}1]$ coalesced over 2.5 μm separation with as little as 0.9 μm OFT growth, while parallel lines with $\theta = 30°$ did not coalesce for this separation and OFT. Using a star-like pattern we examined the coalescence of stripes just off of $\langle 010 \rangle$, each separated by 5.625°. We showed the introduction of a coalescent morphology which differs from the surrounding stripe sidewalls and contributes to the presence or lack of coalescence-related defects, shown in cross-sectional TEM. Two V/III ratios, 124 and 248, were seen to span a range in which complete coalescence could be alternated between those arms having $|\theta| < 45°$ and those having $45° < |\theta| < 90°$. This was attributed to established growth rate anisotropies,

and the observation of possible capillary mass transport at the coalescent region. For both V/III ratios examined under TEM, defects appeared amongst those coalescent regions whose sidewall types were also unfavorable for complete vertical coalescence.

ACKNOWLEDGEMENT

The authors would like to thank DARPA MTO and Intel Corporation for financial support, as well as NNIN and MRL for use of their facilities. The MRL Central Facilities are supported by the MRSEC Program of the NSF under Award No. DMR05-20415; a member of the NSF-funded Materials Research Facilities Network (www.mrfn.org). Funding by DARPA MTO and Intel Corporation.

REFERENCES

1. O. Kayser, R. Westphalen, B. Opitz, and P. Balk, *J. Cryst. Growth* 112, 1 (1991).
2. Z. Yan, Y. Hamaoka, S. Naritsuka, and T. Nishinaga, *J. Cryst. Growth* 212, 1 (2000).
3. H. Asai, *J. Cryst. Growth* 80, 2 (1987).
4. Y.T. Sun, E.R. Messmer, D. Soderstrom, D. Jahan, and S. Lourdudoss, *J. Cryst. Growth* 225, 1 (2001).
5. E. Pelucchi, V. Dimastrodonato, A. Rudra, K. Leifer, E. Kapon, L. Bethke, P.A. Zestanakis, and D.D. Vvedensky, *Phys. Rev. B* 83, 20 (2011).
6. G. Biasiol, F. LeLarge, K. Leifer, and E. Kapon, *J. Cryst. Growth* 195, 1 (1998).
7. M. Ozdemir and A. Zangwill, *J. Vac. Sci. Technol. A* 10, 684 (1992).
8. M. Gibbon, J.P. Stagg, C.G. Cureton, E.J. Thrush, C.J. Jones, R.E. Mallard, R.E. Pritchard, N. Collis, and A. Chew, *Semicond. Sci. Technol.* 8, 6 (1993).
9. F. Lelarge, G. Biasiol, A. Rudra, A. Condo, and E. Kapon, *Microelectron. J.* 30, 4 (1999).